In-Situ Monitoring of Damage Evolution in Glass Matrix Composites during Cyclic Loading using Nondestructive Techniques

E. Z. Kordatos · D. G. Aggelis · K. G. Dassios ·
T. E. Matikas

Abstract Infrared thermography is a powerful non-destructive testing technique which can be used for the detection of damage in advanced materials such as ceramic matrix composites. The purpose of this study is to apply a non-destructive methodology for analyzing, in real-time, the thermal effects in ceramic matrix composites caused by cyclic loading. Mechanical stresses induced by cyclic loading cause heat release in the composite due to failure of the interface, which results in increasing the material's temperature. The heat waves, generated by the thermo-mechanical coupling, and the intrinsic energy dissipated during mechanical cyclic loading of the specimen, were detected by an infrared camera. The results were correlated with acoustic emission events that occurred during the damage accumulation process of the material.

Keywords Glass Matrix Composites · Infrared Thermography · Acoustic Emission · Damage evolution

1 Introduction

The potential of ceramics in advanced high-temperature mechanical applications unfolded significantly after the development, two decades ago, of continuous-fibre-reinforced ceramic matrix composites (CMCs). Such materials offer unique properties to withstand severe thermomechanical loading conditions [1] and are used today in many applications such as aircraft and high-speed vehicle braking systems, structural components, nozzles and thermal barriers in aerospace applications and heat exchangers. CMCs offer notch insensitivity as they can effectively redistribute stresses around notches, voids and cracks. They also show increased crack growth resistance and damage tolerance compared to monolithic ceramics.

E. Z. Kordatos · D. G. Aggelis · K. G. Dassios · T. E. Matikas (✉)
Department of Materials Science &Engineering, University of Ioannina, 45110 Ioannina, Greece
e-mail: matikas@otenet.gr

D. G. Aggelis
Department of Mechanics of Materials and Constructions, Free University of Brussels, Pleinlaan 2, 1050 Brussels, Belgium

These desirable properties stem from the ability of such materials to considerably decrease the catastrophic work available for crack propagation at the crack front by consuming large portions of the externally applied energy in independent mechanisms such as matrix cracking, crack deflection, interfacial damage, fibre bridging, fiber rupture and pull-out [2]. Among the various glass-ceramic matrices of continuous fiber-reinforced ceramic matrix composites (CFCCs), the barium osumilite (BaMg2Al6Si9O30, BMAS:barium-magnesium-alumina-silicate) system [3] is known for its good thermo-physical [4, 5] and mechanical properties [6]. Furthermore, SiC fibres are characterized by high strengths and elastic moduli, thermal stability and great high-temperature mechanical performance. Therefore, SiC fibres provide superior mechanical properties in CMCs [7].

In the aerospace industry inspection is of great significance for all fabrication stages. For this purpose, a fast and reliable nondestructive technique is desirable. Infrared thermography (IRT) can widely satisfy this necessity as a quick, full field and real-time inspection tool. Since the detection depth of IRT is strongly dependent on the investigated material's thermal conductivity, the technique is expected to underperform on ceramic materials and CMCs, compared to conventional metallic matter used in aircraft components [8] and aerospace materials [9]. Nonetheless, the thermal properties of ceramics are sufficient to allow high-precision IRT measurements of flaws and propagating cracks [10].

IRT has been applied in many different materials such as aluminum alloys [11, 12], carbon steels [13], steel fiber concrete [14], metal matrix composites (MMCs) [15] and CMCs [16–18] for damage evaluation. Quantitative thermography has also been used for the rapid assessment of fatigue degradation and of the fatigue limit in materials and structures [19–24] as well as for the evaluation of cumulative damage [25]. Specifically, Muzia et al. [24] developed a relationship between the degree of fatigue degradation and the number of fatigue cycles in epoxy-glass composites. Risitano et al. [25] established a methodology using the thermoanalysis of steel specimen data in order to evaluate the cumulative damage caused by previous loading and for the prediction of the residual life.

Moreover, one of the remarkable advantages of using IRT is that it can detect and monitor sub-surface crack formation and growth. Yang et al. [26] observed the crack propagation and the final fracture by quantifying the temperature evolution during high-cycle fatigue. Furthermore, it has been established that crack growth rate in compact tension specimens can be determined not only with the conventional compliance method but also by thermo-graphic methodologies [15, 27]. Plekhov et al. [28] dealt with the detection, the initiation and the propagation of cracks in 35CrMo4 steel specimens.

Various nondestructive techniques have been combined with IRT for the improved assessment of damage in ceramic composite materials. Particularly, Sfarra et al. [29] used both IRT and holographic interferometry in advanced ceramic materials, while Liu et al. [30] combined electrical resistance acquisition, acoustic emission monitoring and IRT in order to evaluate damage evolution in a 2D C/SiC composite under fatigue loading. Additionally, Reis et al. [31] employed thermographic and acoustic emission techniques to aid the interpretation of fatigue damage mechanisms in glass-fibre-reinforced polypropylene composites.

A separate method used for real time monitoring of the structural integrity of composite materials is acoustic emission (AE). In the most common case, piezoelectric sensors are placed on the surface of the specimen or structure and record the transient stress waves emitted by crack propagation instances [32]. The electric waveforms are stored and analysed in order to provide information on the volumetric density of cracks, as well as the damage condition and crack mode [15, 17, 33, 34]. Due to the usual sequence of fracture mecha-nisms (early tensile cracking precedes ultimate shear) characterization of the cracking mode leads to timely assessment of the material condition offering warning against catastrophic

failure. In general, shear type of cracking (like pull-out, delaminations) have been shown among other characteristics to result to long waveforms with low rising angle, as defined by the ratio of the waveform amplitude over the duration of the initial rising part of the waveform, called "rise time" [12]. An example of this behaviour will be illustrated later, based on the inverse of the rise angle, namely RA value, measured in μs/V.

This work deals with the monitoring of the mechanical behaviour of continuous SiC-fibre reinforced BMAS glass-ceramic matrix composites under cyclic loading. The double-edge notch (DEN) specimen configuration was employed with variable notch-to-width ratio in order to confine material damage resulting to cracking within a pre-determined region. To determine crack initiation and propagation characteristics, this area was monitored by two complementary non-destructive methods, IR thermography and acoustic emission.

2 Experimental Study

2.1 Material

The material examined in this study was a cross-ply SiC/BMAS composite in 3mm thick plate form, processed by AEA Technology (Harwell Ltd, United Kingdom). The reinforcement of glass-ceramic matrix involved silicon carbide fibers, grade "Tyranno" with nominal elastic modulus of 190 GPa and tensile strength of 3.3 GPa (as reported by the manufacturer UBE Industries Ltd., Japan).

Two different notch-to-width ratios (0.2 and 0.35) were prepared in order to study the notch sensitivity of the SiC/BMAS composite. Typical specimens are shown in Fig. 1.

2.2 Experimental Setup

The cyclic loading tests were conducted on an Instron servo-hydraulic frame with maximum static and dynamic load range of ±100 kN. Strain was recorded using an external clip-on axial extensometer.

An infrared (IR) thermographic camera (Cedip) was installed in front of the specimen at a distance of 35 cm in order to attain the optimal field of view (FOV). The IR camera had a cooled indium antimonide (InSb) detector (3–5 μm) and a focal plane array (FPA) with pixel format of 320 (H) × 240 (V). Its sensitivity was 20 mK.

Two acoustic emission sensors (Pico, PAC) were tape-mounted on the same side of the specimen allowing a distance of 40 mm between them as gauge length. Their broadband response, which according to the manufacturer nominally spans frequencies from 200 kHz up to 750 kHz, allowed recording of various acoustic sources. The acquisition sampling rate was 5 MHz, while the threshold was set to 45 dB.
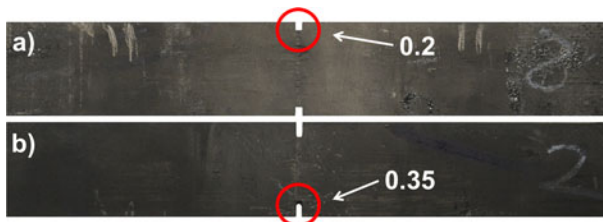

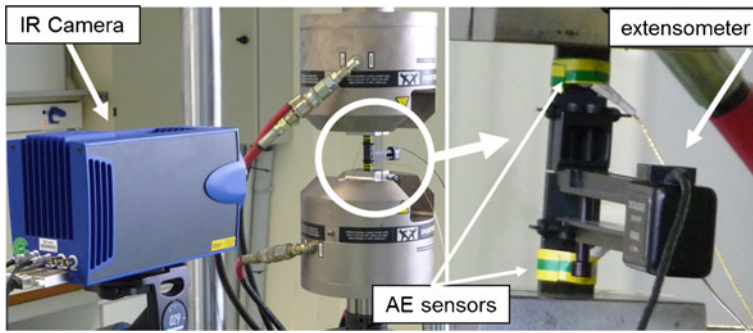**Fig. 1** Double-edge notch (DEN) specimens with variable notch-to-width ratios

Fig. 2 Experimental setup for mechanical testing of double-edge notched composites with simultaneous thermography and acoustic emission monitoring

Figure 2 illustrates a typical arrangement of specimen and equipment (servo-hydraulic machine, infrared camera and specimen with mounted extensometer and AE sensors) during testing.

2.3 Experimental Procedure

Two sets of five specimens, one set for each different notch-to-width ratio, were cyclic loaded until the final fracture. Testing was conducted under displacement control with at a crosshead rate of 0.4 mm/min. Figure 3 shows the recorded load and strain versus time for the 0.2 notch-to-width ratio specimen. Cycles were introduced at displacement intervals of 0.65 mm. At the end of every cycle, the strain and the load were relaxed until the final fracture of the specimen.

3 Results and Discussion

Throughout testing, the surface temperature of the specimens was monitored using IR thermography. Aliasing was avoided by recording the baseline emissivity of the material prior to load application by capturing the IR fingerprint of the surface with the thermal camera. Thermographs were obtained from the area near the notches that exhibited stress concentration (Fig. 4).

Fig. 3 Typical graph of load and strain versus time for 0.2 notch-to-width ratio specimen
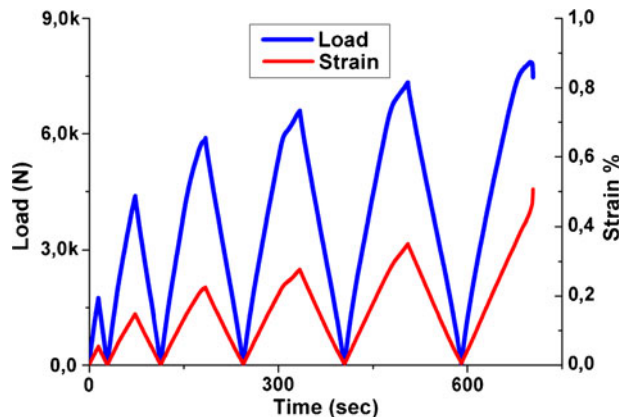
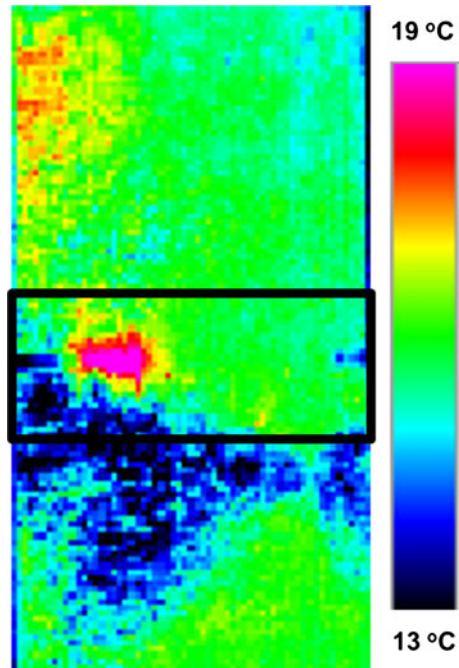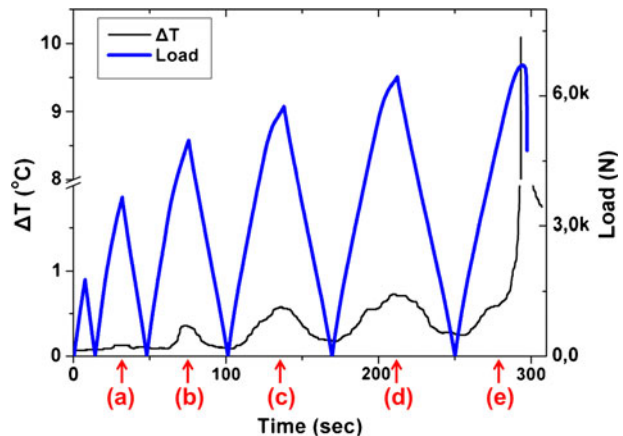**Fig. 4** Typical thermograph of 0.35 notch-to-width ratio specimen

Figure 5 represents ΔT measured by IRT and load as a function of time for two cyclic loading tests on 0.35 notch-to-width ratio specimens. In the time axis, the "a – e" symbols indicate the instances of collection of the thermographs in Fig. 6. As observed in Fig. 5, the peaks of ΔT curve occur at the maximum value of load for every loading cycle. The fact that the ΔT peaks become more obvious from the second loading cycle can be attributed to matrix cracking and the corresponding interfacial damage occurring each time the crack front reaches a new fiber. At the last loading cycle, the ΔT curve does not follow the pattern of the previous cycles involving the temperature increment, reaching the peak and decreasing. Therefore, the curve's slope appears to change abruptly indicating that the specimen is heading for catastrophic fracture.

Fig. 5 Diagram of ΔT and load versus time of cyclic loading for the 0.35 notch-to-width ratio specimen
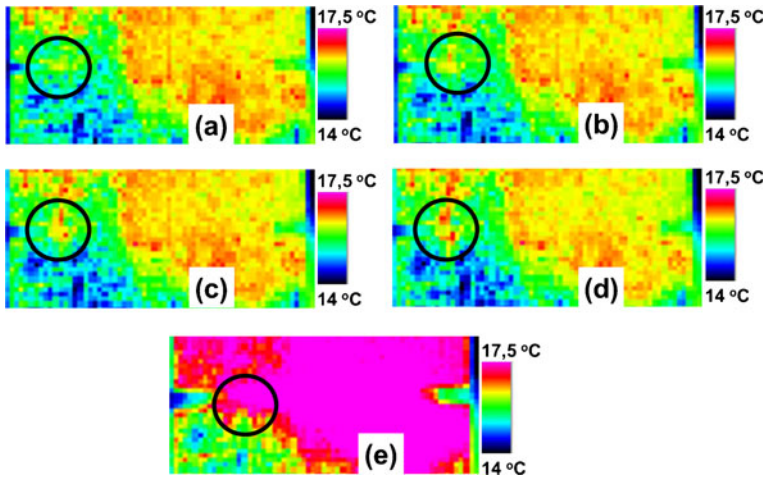
Fig. 6 Thermographs acquired for each loading cycle of the 0.35 notch-to-width ratio specimen

Figure 6 illustrates the thermographs collected at the ΔT curve peaks indicated in Fig. 5. Recalling that the monitored area is near the notches where stress concentration is maximum and the crack initiation occur, the black circles in the thermographs indicate the locations of crack initiation. The area located right of the black circle is a pattern which appears even before the experiment starts and remains the same until the final fracture. This is due to background noise associated with the specimen's surface condition and not with internal damage. In thermograph 6a, corresponding to 32 s experimental time (second loading cycle), there is not noticeable change in temperature. In the third cycle, at 73 s (thermograph 6b), minor temperature variations can be observed within the marked area. Even though they are of small magnitude, they reveal the initiation of damage in the material. This effect becomes more evident in the third thermograph, at 135 s of experimental time. In the thermograph 6d, at 209 s, the variations are clearly increased indicating that damage is extending in area and magnitude. Finally, in the last loading cycle (285 s) a significant temperature increase evidenced through the whole of the monitored area, signifies that specimen fracture is near.

In order to gain a more perspective view about crack propagation, the thermographic monitoring of the final loading cycle in a 0.35 notch-to-width ratio specimen is presented separately (Fig. 7i). The sub-thermographs in Fig. 7i correspond to the loading instances indicated on the diagram of load versus time in Fig. 7ii. As seen in thermograph 7a, there are no hot areas in front of the notches, while in the next thermograph, a clear indication of crack initiation, marked with a red arrow, is observed in front of the left notch. A significant difference in temperature can be seen at 285 s, corresponding to an alteration of the curve's slope. From this time on, the sub-surface crack starts to propagate from the left with direction towards the right notch. Exact knowledge of this instance is critical since it allows the early prediction of final fracture. The associated time (285 s) corresponds to 73% of the final loading step duration. Five seconds later (thermograph 7d) the sub-surface crack has reached the middle of the specimen while only another 300 msec later does it instantly propagate towards the right notch. Further into loading, the specimen attains the maximum temperature (thermograph 7f), which appears at the maximum load of the final cycle (see Fig. 7ii). This maximum temperature is associated with the completion of the matrix cracking procedure and the bearing of the total applied load by the reinforcing SiC-Tyranno fibers. In the next step, thermograph 7g, temperature appears to have decreased
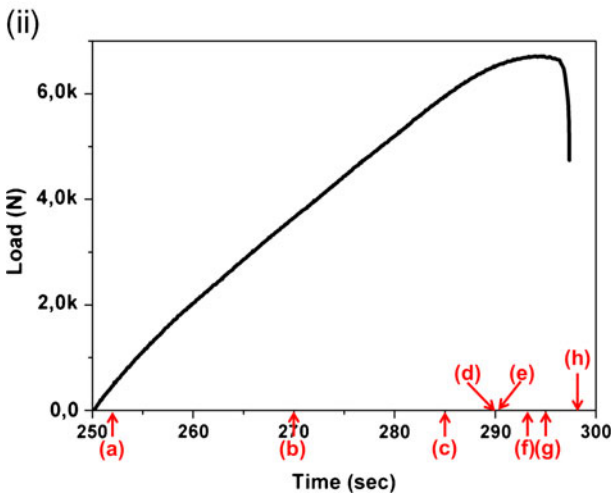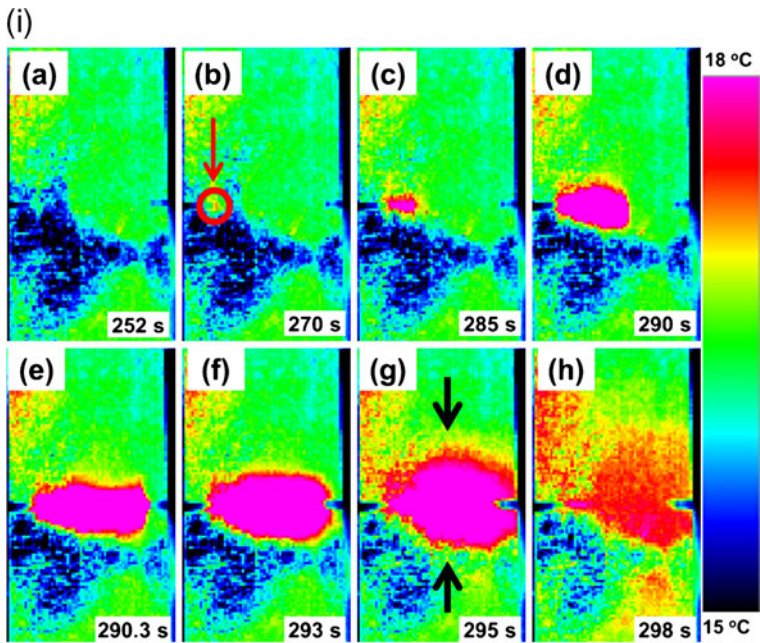
Fig. 7 (i,ii). Thermographs of crack propagation and diagram of load versus time of final loading cycle (0.35 notch-to-width ratio specimen)
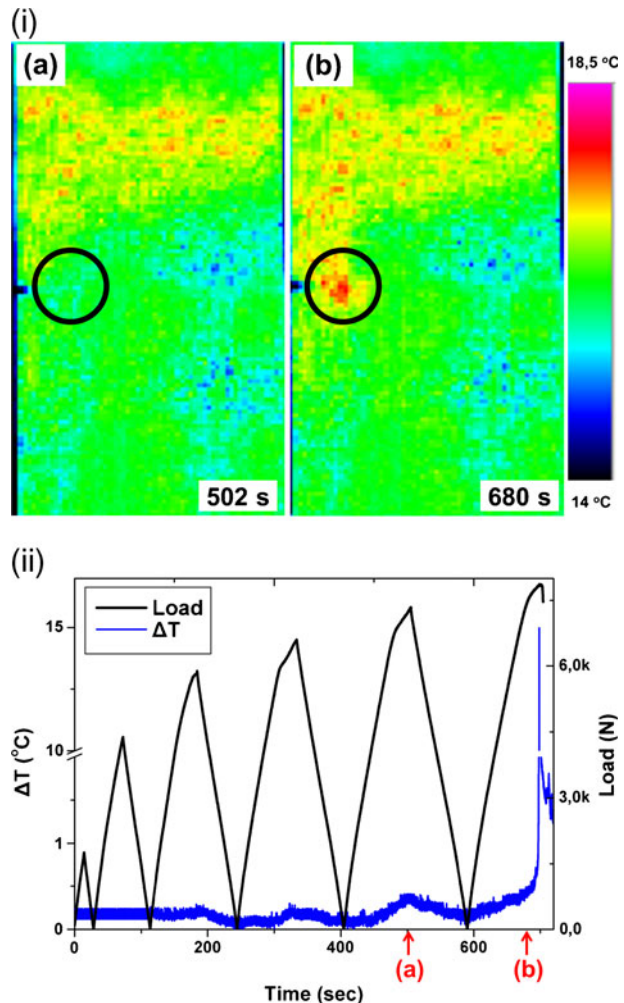
at the left notch, where the crack had initiated, and has increased above and under the subsurface crack, as indicated by black arrows. This effect is related to successive fracture of bridging fibers under the critical levels of instant applied load. Due the progressively decreasing number of surviving fibers, the remaining fibers cannot bear the instant load and fail in a massive manner. This is shown as a significant temperature decrease in the last thermograph. It has to be stressed that even after complete matrix cracking, the SiC fibers resisted separation of the specimen in two pieces, a finding which indicates that the composites underwent extensive pull-out. It must also be noted that the area above the left

notch in Fig. 7h appears to be associated with heat generation due to the stored strain energy and fracture process. The observed effect is, in fact, be due to non-uniform emissivity of the initial surface, as shown in Fig. 7a.

The thermographs and the diagram of load and ΔT as a function of time referring to 0.2 notch-to-width ratio specimen are illustrated in Fig. 8(i, ii). In this case, the thermographs do not present significant temperature variations except of thermograph 8b that corresponds to the final loading cycle. Only indicative thermographs corresponding to the two last cycles of the test are presented. Therefore, as mentioned earlier, thermograph 8a, which relates to 502 s experimental time, does not exhibit obvious temperature increments. On the contrary, at 680 s in thermograph 8b, substantial differences are observed as indicated near the left notch in the marked area, caused by crack initiation.

On the other hand, the diagram of ΔT as a function of time (see Fig. 8ii) is more informative than the thermographs. As can be seen, a minor peak in ΔT curve can be noted even from the third loading cycle. For every loading cycle, the peaks in the ΔT curve occur

Fig. 8 (i,ii). Thermographs and diagram of ΔT and load versus time of cyclic loading for the 0.2 notch-to-width ratio specimen

at maximum load values that are in agreement with those collected in the curves of the 0.35 notch-to-width ratio specimens. In the final loading cycle, the slope of the ΔT curve changes steeply indicating that the specimen is going to fail catastrophically.

As indicated in the thermographs above, the most intense changes can be observed in the final loading cycle. Again, the thermographic monitoring of 0.2 notch-to-width ratio specimen's final loading cycle is analyzed individually in Fig. 9i, in order to assess the crack propagation. The sub-thermographs in Fig. 9i correspond to the loading instances indicated
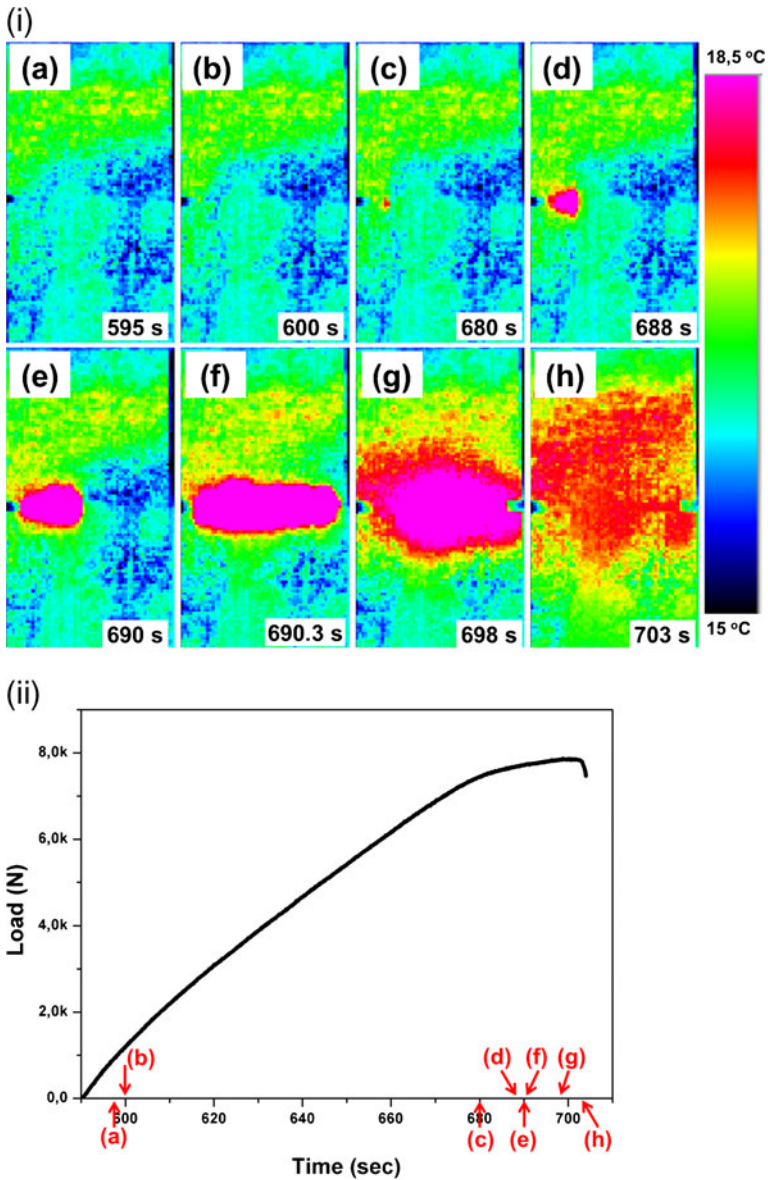

Fig. 9 (i,ii). Thermographs of crack propagation and diagram of load versus time of final loading cycle (0.2 notch-to-width ratio specimen)

on the diagram of load versus time in Fig. 9b. In the thermographs 9a and 9b at 595 s and 600 s respectively, there is no existence of "warm" area near the notches. Crack occurrence is evident in thermograph 9c, which also corresponds to the instance of slope change in the load curve. It is, therefore, possible to predict early fracture at this time, only at 80% of the final loading step duration. Further into loading, in thermographs 9d and 9e, the sub-surface crack propagates starting from the left notch with direction to the middle of the specimen. Next, the sub-surface crack propagates rapidly to the right notch due to instable crack growth in the matrix. At the last thermograph, 9h, no temperature variations are seen and the specimen fails without being separated into two pieces.

In Fig. 10, the peaks of the ΔT curves are illustrated for both notch length used in this study. It is observed that the specimen with smaller notches exhibit 15 °C ΔT at the fracture, while the 0.35 notch-to-width ratio specimen reaches only 10 °C ΔT. This finding is not unreasonable if the different lengths of notched ligaments of the two specimens are considered. In specimens with larger notched ligaments (smaller notches), damage evolves over a wider material region throughout testing hence peak temperature at the critical load is high. On the other hand, damage is accumulated and relieved not so drastically in a specimen with less material available within the notched region.

Material damage was also monitored by acoustic emission. In Fig. 11, the RA-value curve is presented with respect to time as well as the ΔT values. RA is defined as the ratio of the rise time over the peak amplitude of the AE waveform and is measured in $\mu s/V$ [34], see the embedded graph of Fig. 11. The RA line is the moving average of the recent 70 points. It is clear that the RA line exhibits high peaks at the moments of high strain for each cycle. These peaks are associated with clear ΔT peaks. At low strains the average RA is limited under 1,000 $\mu s/V$. On the contrary, when strain increases, approximately in the middle of each cycle, RA exhibits sharp peaks over 10,000 $\mu s/V$. This reveals the higher intensity occurrences which are triggered by the high level of load and implies that the nature of these events is different than the ones exhibited at low strain. It is known that high values of RA are connected to shear mode of fracture either due to pure shear stresses of phenomena like delamination and fiber pull-out in different materials [12, 35]. The peaks of RA coincide with the local maxima of temperature. As argued earlier, increased stress in the material has an effect of heating. At the same time however, high levels of stress induce higher intensity

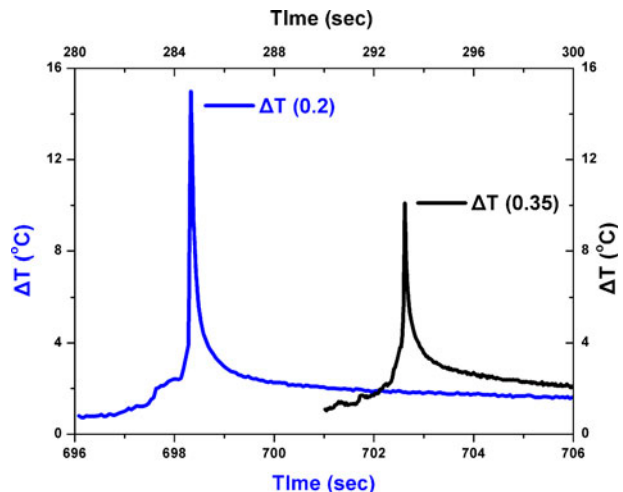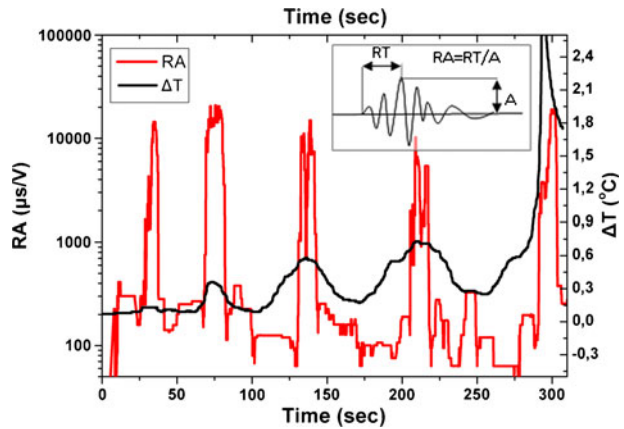Fig. 10 Peaks of the ΔT curves for both types of notches

Fig. 11 Time histories of AE RA and ΔT. (The RA line is the moving average of the recent 70 individual points. In the embedded figure the RA of a typical waveform is illustrated)

damage mechanisms resulting in changes of acoustic emission signatures as shown by the RA fluctuations in Fig. 11.

4 Conclusion

In this paper, thermographic analysis was correlated with acoustic emission signals for the determination of crack initiation and propagation characteristics leading to final fracture of the specimen. Infrared thermography, as a full-field and real-time technique, was employed to identify crack initiation, both in location and in time, as well as to monitor the crack propagation path during mechanical testing of a SiC-fiber reinforced ceramic matrix composite. Successfull application of the technique under such dynamic conditions where the surface changes with usage is close to real-life scenarios found in structures such as aircraft or ground transport vehicles. It is implied that application of the technique to a static structure is a much less demanding task that can be trivially achieved by simple downscaling of the proposed technique. IR thermography results also enabled early prediction of the residual life of ceramic matrix composites, at 73% of the duration of the final loading step. Based on the results, it can be concluded that IR thermography is a useful tool for the determination of damage and crack propagation in ceramic matrix composites.

Complimentarily, recording of the acoustic emission behavior of the material offers the potential to characterize the condition of the material as load varies and the shift between different fracture mechanisms, while further study should be conducted for the accurate characterization of the different failure modes.

References

1. Evans, A.G.: The mechanical performance of fiber-reinforced ceramic matrix composites. Mater Sci Eng, A **107**, 227–239 (1989). doi:10.1016/0921-5093(89)90391-2
2. Dassios, K.G.: Energy dissipation in ceramic matrix composites: direct measurement and phenomenological assessment. J Eng Technol **1**(3), 44–56 (2011)
3. Brennan JJ, C.K., Taylor M.P.: High strength thermally stable magnesium aluminosilicate glass ceramic matrix SiC fibre composite
4. Johnson, L.F., Hasselman, D.P.H., Chyung, K.: Effect of silicon-carbide fiber or whisker reinforcement on the thermal-diffusivity conductivity of an osumilite glass-ceramic. J Am Ceram Soc **70**(6), C135–C138 (1987)

5. Yilmaz, R., Taylor, R.: Effect of heat treatment in air on the thermal properties of SiC fibre-reinforced composite. Part 1: a barium osumilite (BMAS) matrix glass ceramic composite. J Mater Sci **42**(3), 763–771 (2007). doi:10.1007/s10853-006-1443-3

6. Choy, K.L., Duplock, P., Rogers, P.S., Churchman-Davies, J., Pirzada, M.T.: The mechanical behaviour of glass and glass-ceramic matrix composites. Mat Sci Eng a-Struct **278**(1–2), 187–194 (2000)

7. Brennan, J.J., Prewo, K.M.: Silicon carbide fibre reinforced glass-ceramic matrix composites exhibiting high strength and toughness. J Mater Sci **17**(8), 2371–2383 (1982). doi:10.1007/bf00543747

8. Bates, D., Smith, G., Lu, D., Hewitt, J.: Rapid thermal non-destructive testing of aircraft components. Compos Part B: Eng **31**(3), 175–185 (2000). doi:10.1016/s1359-8368(00)00005-6

9. Avdelidis, N.P., Hawtin, B.C., Almond, D.P.: Transient thermography in the assessment of defects of aircraft composites. NDT and E Int **36**(6), 433–439 (2003). doi:10.1016/s0963-8695(03)00052-5

10. Mei, H.: Current development in non-destructive testing and damage evaluation for ceramic matrix composites. Adv Appl Ceram **108**(2), 84–91 (2009). doi:10.1179/174367608x378569

11. Kordatos, E.Z., Aggelis, D.G., Matikas, T.E.: Monitoring of fatigue damage in metal plates by acoustic emission and thermography, vol. 7982. vol. 1. SPIE, (2011)

12. Aggelis, D.G., Kordatos, E.Z., Matikas, T.E.: Acoustic emission for fatigue damage characterization in metal plates. Mech Res Commun **38**(2), 106–110 (2011). doi:10.1016/j.mechrescom.2011.01.011

13. Kordatos, E.Z., Matikas, T.E.: Developing damage metrics for metallic structures undergoing fatigue using real-time thermographic evaluation, vol. 7982. vol. 1. SPIE, (2011)

14. Aggelis, D.G., Kordatos, E.Z., Soulioti, D.V., Matikas, T.E.: Combined use of thermography and ultrasound for the characterization of subsurface cracks in concrete. Constr Build Mater **24**(10), 1888 (2010)

15. Kordatos, E.Z., Aggelis, D.G., Matikas, T.E.: Monitoring mechanical damage in structural materials using complimentary NDE techniques based on thermography and acoustic emission. Composites Part B: Engineering(0). doi:10.1016/j.compositesb.2011.12.013

16. Kim, J., Liaw, P.K.: Tensile Fracture Behavior of Nicalon/SiC Composites. Metall Mater Trans A **38**(13), 2203–2213 (2007). doi:10.1007/s11661-007-9306-3

17. Dassios, K.G., Aggelis, D.G., Kordatos, E.Z., Matikas, T.E.: Cyclic loading of a SiC-fiber reinforced ceramic matrix composite reveals damage mechanisms and thermal residual stress state. Compos Part A: Appl Sci Manuf **44**, 105–113 (2013). doi:10.1016/j.compositesa.2012.06.011

18. Kordatos, E.Z., Aggelis, D.G., Dassios, K.G., Lagari, P.L.I., Matikas, T.E.: Real-time characterization of damage in ceramic matrix composites using IR thermography and acoustic emission. In: Proc. SPIE 8346 "Smart Sensor Phenomena, Technology, Networks, and Systems Integration", San Diego CA 2012, p. 834617

19. Brémond, P., Potet, P.: Lock-in thermography: A tool to analyse and locate thermo-mechanical mechanisms in materials and structures. In: Rozlosnik, A.E., Dinwiddie, R.B. (eds.), Orlando, FL 2001. Thermosense XXIII, pp. 560-566

20. Minh Phong, L.: Fatigue limit evaluation of metals using an infrared thermographic technique. Mech Mater **28**(1–4), 155–163 (1998). doi:10.1016/s0167-6636(97)00047-1

21. Krapez, J.C., Pacou, D., Gardette, G.: Lock-in thermography and fatigue limit of metals. Proc. QIRT'2000, 277-282 (2000)

22. La Rosa, G., Risitano, A.: Thermographic methodology for rapid determination of the fatigue limit of materials and mechanical components. Int J Fatigue **22**(1), 65–73 (2000). doi:10.1016/s0142-1123(99)00088-2

23. Kordatos, E.Z., Strantza, M.A., Dassios, K.G., Lagari, P.L.I., Matikas, T.E.: Determination of fatigue limit in composite materials using IR lock-in thermography. In: DURACOSYS 2012, 10th International Conference on Durability of Composite Systems, Brussels (2012)

24. Muzia, G., Rdzawski, Z.M., Rojek, M., Stabik, J., Wróbel, G.: Thermographic diagnosis of fatigue degradation of epoxy-glass composites. Journal of Achievements in Materials and Manufacturing Engineering **24**(2) (2007)

25. Risitano, A., Risitano, G.: Cumulative damage evaluation of steel using infrared thermography. Theor Appl Fract Mech **54**(2), 82–90 (2010). doi:10.1016/j.tafmec.2010.10.002

26. Yang, B., Liaw, P.K., Wang, G., Peter, W.H., Buchanan, R.A., Yokoyama, Y., Huang, J.Y., Kuo, R.C., Huang, J.G., Fielden, D.E., Klarstrom, D.L.: Thermal-Imaging Technologies for Detecting Damage during High-Cycle Fatigue. Metall Mater Trans A: Phys Metall Mater Sci **35 A**(1), 15–23 (2004)

27. Ait Aouit, D., Ouahabi, A.: Monitoring crack growth using thermography. Suivi de fissuration de matériaux par thermographie **336**(8), 677–683 (2008). doi:10.1016/j.crme.2008.06.001

28. Plekhov, O., Palin-Luc, T., Saintier, N., Uvarov, S., Naimark, O.: Fatigue crack initiation and growth in a 35CrMo4 steel investigated by infrared thermography. Fatigue Fract Eng Mater Struct **28**(1–2), 169–178 (2005). doi:10.1111/j.1460-2695.2004.00837.x

29. Sfarra, S., Ibarra-Castanedo, C., Bendada, A., Maldague, X., Ambrosini, D., Paoletti, D.: Comparative study for the nondestructive testing of advanced ceramic materials by infrared thermography and holographic interferometry. In, Orlando, FL 2010. Thermosense XXXII

30. Liu, C., Cheng, L., Luan, X., Li, B., Zhou, J.: Damage evolution and real-time non-destructive evaluation of 2D carbon-fiber/SiC-matrix composites under fatigue loading. Mater Lett **62**(24), 3922–3924 (2008). doi:10.1016/j.matlet.2008.04.063

31. Reis, P., Ferreira, J., Richardson, M.: Fatigue damage characterization by NDT in polypropylene/glass fibre composites. Appl Compos Mater **18**(5), 409–419 (2011). doi:10.1007/s10443-010-9172-9

32. Trojanová, Z., Száraz, Z., Chmelík, F., Lukáč, P.: Acoustic emission from deformed Mg–Y–Nd alloy and this alloy reinforced with SiC particles. J Alloys Compd **504**(2), L28–L30 (2010). doi:10.1016/j.jallcom.2010.05.138

33. Grosse, C., Reinhardt, H., Dahm, T.: Localization and classification of fracture types in concrete with quantitative acoustic emission measurement techniques. NDT & E Int **30**(4), 223–230 (1997). doi:10.1016/s0963-8695(96)00060-6

34. Carpinteri, A., Lacidogna, G., Niccolini, G., Puzzi, S.: Critical defect size distributions in concrete structures detected by the acoustic emission technique. Meccanica **43**(3), 349–363 (2008). doi:10.1007/s11012-007-9101-7

35. Aggelis, D.G., Soulioti, D.V., Barkoula, N.M., Paipetis, A.S., Matikas, T.E.: Influence of fiber chemical coating on the acoustic emission behavior of steel fiber reinforced concrete. Cem Concr Compos **34**(1), 62–67 (2012). doi:10.1016/j.cemconcomp.2011.07.003